



Frequency uncertainty improvement in a STFT-BOTDR using highly nonlinear optical fibers

LINQING LUO,¹ FRANCESCA PARMIGIANI,² YIFEI YU,¹ BO LI,¹ KENICHI SOGA³ AND JIZE YAN^{4*}

¹Engineering Department, University of Cambridge, Cambridge, CB2 1PZ, UK

²Optoelectronics Research Centre, University of Southampton, SO17 1BJ, UK

³Department of Civil and Environmental Engineering, University of California-Berkeley, Berkeley, California, 94720, USA

⁴Electronics and Computer Science, University of Southampton, Southampton, SO17 1BJ, UK

*J.yan@soton.ac.uk

Abstract: The sensitivity of a sensor to strain or the temperature variations due to distributed Brillouin scattering are partially related to the type of fibers used and the Brillouin scattering induced effective index. In this paper, a highly nonlinear fiber that can generate a higher Brillouin scattering signal is compared to a standard single mode fiber in a short-time-Fourier-transform Brillouin optical time domain reflectometer (STFT-BOTDR). The results show that much higher signal to noise ratios of the Brillouin scattering spectrum and smaller frequency uncertainties in the sensing measurement can be achieved in the highly nonlinear fiber for comparable launched powers. With a measurement speed of 4 Hz, the frequency uncertainty can be 0.43 MHz, corresponding to 10 $\mu\epsilon$ in strain or 0.43°C in temperature uncertainty for the highly nonlinear fiber. In contrast, for the standard single mode fiber case, the value would increase to about 1.02 MHz (25 $\mu\epsilon$ or 1.02°C), demonstrating the advantage of the highly nonlinear fiber for distributed strain/temperature sensing.

Published by The Optical Society under the terms of the [Creative Commons Attribution 4.0 License](#). Further distribution of this work must maintain attribution to the author(s) and the published article's title, journal citation, and DOI.

OCIS codes: (060.2370) Fiber optics sensors; (060.4370) Nonlinear optics, fibers.

References and links

1. X. Bao and L. Chen, "Recent progress in Brillouin scattering based fiber sensors," *Sensors (Basel)* **11**(12), 4152–4187 (2011).
2. L. Thévenaz, "Brillouin distributed time-domain sensing in optical fibers: State of the art and perspectives," *Front. Optoelectron. China* **3**(1), 13–21 (2010).
3. C. A. Galindez-Jamioy and J. M. López-Higuera, "Brillouin distributed fiber sensors: an overview and applications," *J. Sens.* **2012**, 1–17 (2012).
4. T. Horiguchi, K. Shimizu, T. Kurashima, M. Tateda, and Y. Koyamada, "Development of a distributed sensing technique using Brillouin scattering," *J. Lightwave Technol.* **13**(7), 1296–1302 (1995).
5. A. Motil, A. Bergman, and M. Tur, "State of the art of Brillouin fiber-optic distributed sensing," *Opt. Laser Technol.* **78**(A), 81–103 (2016).
6. S.-B. Cho, Y.-G. Kim, J.-S. Heo, and J.-J. Lee, "Pulse width dependence of Brillouin frequency in single mode optical fibers," *Opt. Express* **13**(23), 9472–9479 (2005).
7. L. Luo, B. Li, Y. Yu, X. Xu, K. Soga, and J. Yan, "Time and frequency localized pulse shape for resolution enhancement in STFT-BOTDR," *J. Sens.* **2016**, 10 (2016).
8. C. Kechavarzi, K. Soga, N. Battista, L. Pelecanos, M. Elshafie, and R. Mair, *Distributed Fibre optic Strain Sensing for Monitoring Civil Infrastructure, 1st Edition* (London: ICE Publishing, 2016).
9. X. Liu and X. Bao, "Brillouin spectrum in LEAF and simultaneous temperature and strain measurement," *J. Lightwave Technol.* **30**(8), 1053–1059 (2011).
10. Y. Mizuno, N. Hayashi, and K. Nakamura, "Brillouin scattering in plastic optical fibers: Fundamental properties and sensing applications," *Photonics Global Conference*, Singapore, Singapore, 13–16 Dec, 2012.
11. B. Stiller, *Brillouin Scattering in Photonic Crystal Fiber: From Fundamentals to Fiber Optic Sensors*, English (Universit'e de Franche-Com'te, 2013).

12. M. J. Holmes, D. Williams, and R. Manning, "Highly nonlinear optical fiber for all optical processing applications," *IEEE Photonics Technol. Lett.* **7**(9), 1045–1047 (1995).
13. L. Grüner-Nielsen, S. Dasgupta, M. D. Mermelstein, D. Jakobsen, S. Herstrøm, M. E. V. Pedersen, E. L. Lim, S.-u. Alam, F. Parmigiani, D. Richardson, and B. Pálsdóttir, *A Silica Based Highly Nonlinear Fiber with Improved Threshold for Stimulated Brillouin Scattering* (Torino, 2010).
14. J. H. Lee, T. Tanemura, K. Kikuchi, T. Nagashima, T. Hasegawa, S. Ohara, and N. Sugimoto, "Experimental comparison of a Kerr nonlinearity figure of merit including the stimulated Brillouin scattering threshold for state-of-the-art nonlinear optical fibers," *Opt. Lett.* **30**(13), 1698–1700 (2005).
15. G. P. Agrawal, *Nonlinear Fiber Optics, Fifth Edition* (Oxford: Academic Press, 2007).
16. J. H. Lee, W. Belardi, K. Furusawa, P. Petropoulos, P. Yussuff, T. Monro, and D. Richardson, "Four-wave mixing based 10-Gb/s tunable wavelength conversion using a holey fiber with a high SBS threshold," *IEEE Photonics Technol. Lett.* **15**(3), 440–442 (2003).
17. J. Hansryd, F. Dross, M. Westlund, P. A. Andrekson, and S. Knudsen, "Increase of the SBS threshold in a short highly nonlinear fiber by applying a temperature distribution," *J. Lightwave Technol.* **19**(11), 1691–1697 (2001).
18. J. M. Chavez Boggio, J. D. Marconi, and H. L. Fragnito, "Experimental and numerical investigation of the SBS-threshold increase in an optical fiber by applying strain distributions," *J. Lightwave Technol.* **23**(11), 3808–3814 (2005).
19. B. Li, L. Luo, Y. Yu, K. Soga, and J. Yan, "Dynamic strain measurement using small gain stimulated Brillouin scattering in STFT-BOTDR," *IEEE Sens. J.* **17**(9), 2718–2724 (2017).
20. A. Kobaykov, M. Sauer, and D. Chowdhury, "Stimulated Brillouin scattering in optical fibers," *Adv. Opt. Photonics* **2**(1), 1–59 (2010).
21. R. G. Smith, "Optical power handling capacity of low loss optical fibers as determined by stimulated Raman and Brillouin scattering," *Appl. Opt.* **11**(11), 2489–2494 (1972).
22. I. Malitson, "Interspecimen comparison of the refractive index of fused silica," *J. Opt. Soc. Am.* **55**(11), 1205–1208 (1965).
23. D. Royer and E. Dieulesaint, *Ondes Elastiques Dans Les Solides* (Dunod, 1997).
24. P. Benassi, V. Mazzacurati, G. Ruocco, and G. Signorelli, "Elasto-optic constants in silicate glasses: Experiment and theory," *Phys. Rev. B Condens. Matter* **48**(9), 5987–5996 (1993).
25. Y. Yu, L. Luo, B. Li, K. Soga, and J. Yan, "Frequency resolution quantification of Brillouin distributed optical fiber sensors," *IEEE Photonics Technol. Lett.* **28**(21), 2367–2370 (2016).
26. Y. Yu, L. Luo, B. Li, K. Soga, and J. Yan, "Quadratic time-frequency transforms-based Brillouin optical time-domain reflectometry," *IEEE Sens. J.* **17**(20), 6622–6626 (2017).
27. O. Aso, M. Tadakuma, and S. Namiki, "Four-wave mixing in optical fibers and its applications," *Furukawa Review* **19**, 63–68 (2000).
28. R. H. Stolen and C. Lin, "Self-phase-modulation in silica optical fibers," *Phys. Rev. A* **17**(4), 1448–1453 (1978).
29. G. Agrawal and A. Olsson, "Self-phase modulation and spectral broadening of optical pulses in Semiconductor Laser Amplifiers," *IEEE J. Quantum Electron.* **25**(11), 2297–2306 (1989).

1. Introduction

Distributed fiber optic sensing (DFOS) has attracted increasing engineering interest due to its capability for accurate monitoring of the strain and temperature values over long distances. It has significant advantages in obtaining a continuous signal compared to point sensors [1]. As a DFOS technique, the Brillouin optical time domain reflectometer (BOTDR) has the advantage of requiring the access to only one end of the optical fiber, and has become widely adopted by civil engineers for use in structural health monitoring (SHM) [2, 3]. Brillouin frequency shift (BFS) is the shift in frequency between the peak of the sharp Brillouin gain spectrum of the scattered signal generated along the fiber under test (FUT) and the pump laser spectrum seeding the process and propagating in the opposite direction of the FUT [4]. BOTDR measures the changes of the BFS along the FUT.

The sensitivity of a sensor to strain or temperature variations is related to its strain or temperature resolution and this is proportional to the uncertainty in frequency of the Brillouin scattering spectrum peak [5], which is linearly influenced by the local Brillouin scattering coefficient of the fiber. In the BOTDR, this frequency uncertainty is limited by inherently weak spontaneous Brillouin scattering, reducing the signal to noise ratio (SNR) of the detected signal. Consequently, the number of average used in each measurement is increased to reduce the impact of the noise. Increasing the pulse width of the seed can improve its scattering spectrum peak power, albeit at the expense of lowering the spatial resolution [6]. An optimized pulse shape can also improve the SNR of the Brillouin scatter spectrum to some extent by having a smaller full width at half maximum (FWHM) [7].

Recently different fibers have been used, each with different advantages and limitations [8]. Large effective area fibers are used to achieve simultaneous temperature and strain measurements [9], while Polymer fibers have the potential for high-accuracy temperature sensing [10]. Photonic crystal fibers with their large nonlinear coefficients can generate high Brillouin spectrum gains, but their large structural irregularities along their lengths limit their performance in distributed sensing [11].

Commercially available highly nonlinear fibers (HNLFs) with high degree of uniformity along their lengths are interesting solutions as they guarantee high Brillouin gain spectrum, thus, enhancing the Brillouin scattering signal and improving the resolution of the system. In this paper, a HNLF is tested in a STFT-BOTDR system. The SNR of the Brillouin spectrum and frequency uncertainty are compared to those of a standard telecom single mode fiber (SMF-28).

2. Highly nonlinear fiber

Dispersion shifted HNLFs have high nonlinear coefficients, γ , (typically 10-20/W/km) with dispersion coefficients close to zero [12]. To increase their nonlinear coefficient value, higher nonlinear refractive indexes or smaller effective areas to tightly confine the light in the core are typically used [13]. They have been widely adopted in many nonlinear signal processing applications such as optical switches, sampling, wavelength conversion, gain amplification, pulse compression, etc [14]. The power that can be launched into the fiber is limited by Stimulated Brillouin Scattering (SBS) in continuous wave (CW) -pump applications, and can be expressed as [14, 15]:

$$\gamma L_{eff} P_{th} \propto \frac{n_2}{g_B} \quad (1)$$

where L_{eff} is the effective length [16], P_{th} is the threshold power for the SBS which is the power where the SBS builds up almost exponentially [15], n_2 is the nonlinear refractive index, and g_B is the Brillouin gain coefficient of the fiber. In those applications, methods to suppress the SBS threshold are proposed, for example, by inducing linear or stepwise temperature [17] or linear strain [18] gradients along their lengths, or using other doping materials, such as aluminium (Al) instead of germanium (Ge) in the fiber core [14].

Due to the lower SBS threshold, HNLFs generate stronger Brillouin scattering for the same incident seed power. This leads to higher SNR of the Brillouin scattering signal and smaller number of averages, suggesting that HNLF-BOTDRs are more suitable for dynamic measurements [19].

3. Theoretical calculation

By carefully selecting the parameters of a HNLF, the Brillouin scattering power can be stronger than the one of the typical SMF-28 which is currently the dominant fiber used in the distributed fiber optic systems both in laboratory or civil, oil and gas industry.

3.1 Brillouin scattering improvement with nonlinear fiber

The SBS is an amplifying process with a Brillouin gain factor. For a single mode fiber, and for one polarization direction, the peak Brillouin gain factor can be expressed by [11, 20]

$$g_B = \frac{4\pi n^8 p_{12}^2}{c \lambda_p^2 \rho_o \nu_B \Delta \nu_B} \quad (2)$$

where n is the effective refractive index, p_{12} is the respective component of the electrostriction tensor, c is the speed of light in vacuum, λ_p is the wavelength of the pump

light, ρ_o is the mean density of the material of the fiber, ν_B is the frequency shift of the BGS, and $\Delta\nu_B$ is the FWHM width of the BGS.

From Eq. (2), the doping of the fiber can change ν_B and $\Delta\nu_B$ as previously discussed. However, due to the small doping concentration of Germanium and Aluminium than silica in the optical fiber, its density, electrostriction tensor, and refractive index will not be significantly changed (the main contribution is still silica). The threshold power in Eq. (1) can be further written as [11, 20].

$$P_{TH} = \frac{CKA_{eff}}{g_B L_{eff}} \quad (3)$$

where C is the coefficient of the Stimulated Brillouin Scattering criteria and is typically assumed to be 21 [21], K represents for random polarization evolution in the fiber and normally equals to 3/2, and A_{eff} is the effect area of the fiber core.

The large Brillouin peak powers achieved for the HNLF case will lead to large SNR [19] as shown in Eq. (4).

$$SNR(dB) = 10 \log_{10} \left(\frac{2R^2 P_B P_{OLO} \sqrt{N}}{4kTB / R_L + 2eRP_{OLO}B + (RP_{OLO})^2 RIN B} \right) - NF_{E-noise} \quad (4)$$

where R is the responsivity of the photodetector, P_B is the Brillouin scattering power, P_{OLO} is the power of the local oscillator branch from the laser, N is the number of averaging, k is the Boltzmann constant, T is the temperature, B is the detected bandwidth, R_L is the load resistance, e is the electron charge, RIN is the relative intensity noise, and $NF_{E-noise}$ is the total noise figure of electronic components.

From Eq. (2) and Eq. (3), it is possible to select HNLFs with lower SBS threshold powers than the ones of SMF, hence with larger Brillouin scattering signal powers. The parameters to calculate the Brillouin gain are listed in Table 1 [11]:

Table 1. The values of the parameters to calculate Brillouin gain

Refractive index silica	$n = 1.44$ [22]
Elasto-optic constant of SiO ₂	$p_{12} = 0.285$ [23]
Density	$\rho_o = 2.21 \times 10^3 \text{ kg / m}^3$ [24]
Wavelength of pump incident light	$\lambda_p = 1554.13 \text{ nm}$
Acoustic velocity	$V_A = 5996 \text{ m/s}$ [23]

The parameters of the used HNLF, named as HNLF-1145A, are shown in Table 2 together with the ones of a SMF.

Table 2. The parameters of SMF-28 and HNLF-1145A

	SMF	HNLF-1145A
FWHM ($\Delta\nu_B$)	100 MHz	50 MHz
Effective area (A_{eff})	80 μm^2	10.5 μm^2
Centre frequency for BGS (ν_B)	10.8 GHz	9.6 GHz
Attenuation (α)	0.2 dB/km	0.59 dB/km

By substituting the parameters in *Table 1* and *Table 2* into Eq. (2) and Eq. (3), and assuming the effective length is equal to the fiber length (1 km), the SBS threshold of SMF-28 is approximately 58.1 mW (17.6 dBm), while the SBS threshold of HNLF-1145A is 4.6 mW (6.62 dBm). Therefore, the SBS threshold of HNLF is about 11 dB smaller than the one of the SMF; the Brillouin signal power is stronger in the HNLF case than in the SMF case.

The FWHM of the Brillouin scattered spectrum was 50 MHz for HNLF-1145A, and 100 MHz for SMF-28. For practical purposes, the two frequencies of the Brillouin scattered spectrum peaks for the two fibers are down-converted to the same value by adjusting the VCO in the detecting electronics. Narrower spectral FWHMs give larger Q-factor and as a result, smaller frequency uncertainty, σ , in the sensing system [25, 26]:

$$Q = \frac{v_B}{FWHM} \quad (5)$$

$$\sigma \approx \frac{v_B \times \delta^{0.05}}{8.5 \times Q \times SNR^{0.25}} \quad (6)$$

where v_B is the down-converted BFS, and δ is the frequency step resolution, which is determined by the number of data points and the sampling rate in the DFT system, and is the frequency sweeping step in the frequency sweeping system.

3.2 Experiment on the Brillouin scattering power improvement

To test the relationship between the incident pump power and the Brillouin Scattering power, HNLF-1145A is characterized and referred to as the fiber under test (FUT) in Fig. 1. HNLF-1145A had a dispersion at 1550nm of + 0.32 ps/nm/km, a polarization-mode dispersion (PMD) of 0.03 ps/rkm, while all the other parameters are reported in *Table 2*.

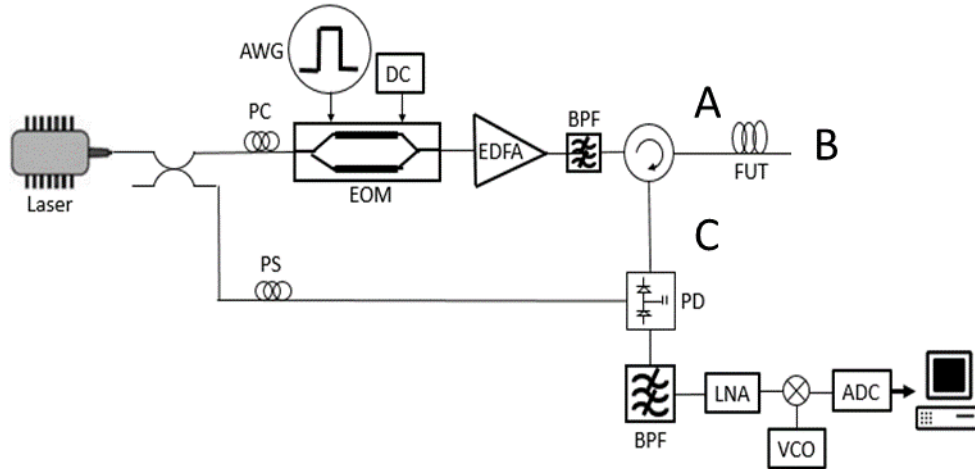


Fig. 1. Experimental set-up of the STFT-BOTDR to test the HNLF-1145A and SMF-28. AWG: arbitrary waveform generator; EOM: electro-optic modulator; BPF: DWDM filter; PS: polarization scrambler; PD: photodiode; BPF: bandpass filter; LNA: low noise amplifier; VCO: voltage controlled oscillator ADC: analogue to digital converter.

A narrow-line-width laser with wavelength of 1554.13 nm was used as the pump source. A part of the continuous-wave (CW) light was modulated by an electro-optic modulator (EOM) generating optical pulses with FWHM of 20 ns and repetition rate of 50 kHz, using an Arbitrary Wave Generator (AWG, Agilent 33600). The pulses were then amplified by an Erbium-doped fiber amplifier (EDFA). The amplified signal was then filtered by a 100 GHz

optical filter, and launched into the FUT via a circulator to generate the Brillouin backscattered signal. The HNLF is connected to the SMF of the circular where the coupling loss between the SMF and HNLF is negligible, about 0.2 dB. The powers at the following three points were recorded: at the input (point A) and output (point B) of the FUT, and after port 3 of the circulator (point C). They are plotted in Fig. 2.

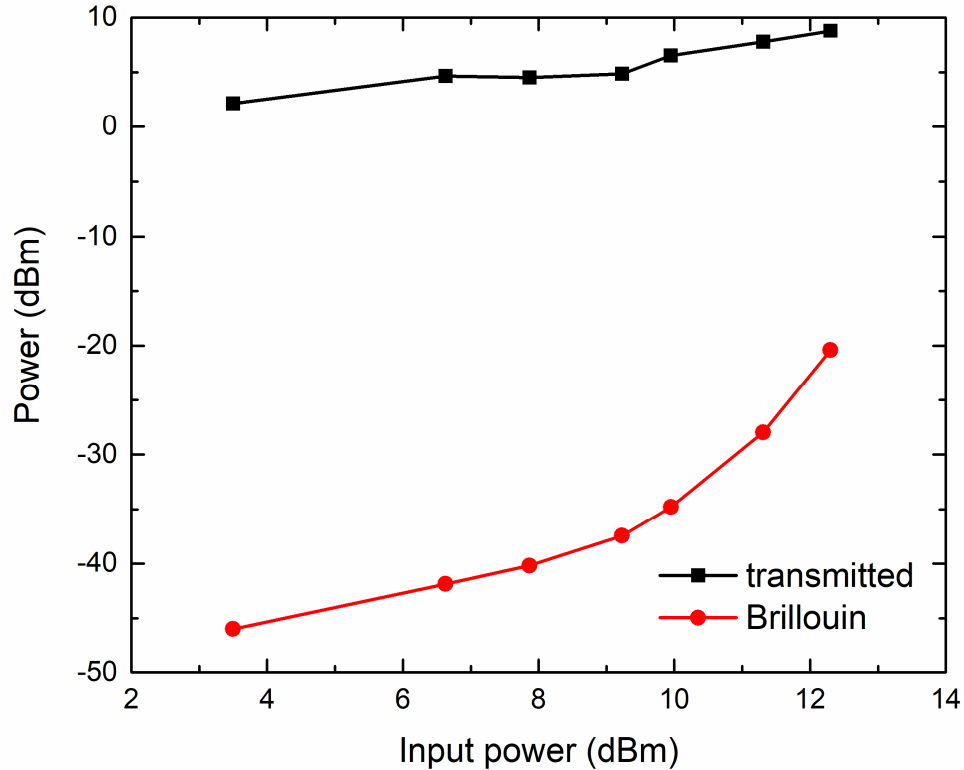


Fig. 2. Transmitted and back reflected Brillouin powers as a function of input power for HNLF-1145A.

The Brillouin scattering power is measured at the peak frequency slot of the Brillouin spectrum from the optical spectrum analyzer, while the incident and transmitted powers are measured at the central wavelength of the CW source, i.e. at 1554.13 nm. Figure 2 shows that, when the incident pump power (average power) is as low as 3.5 dBm, the transmitted and Brillouin scattered powers are 3 dBm and -46 dBm, respectively. As the incident power increases, the transmitted power saturates at 5 dBm, while the Brillouin scattering power increases rapidly. From Fig. 2, when the incident pump power is about 15 dBm, the Brillouin scattering power can be predicted to be identical to the transmitted one and above that the Brillouin scattering power is greater than transmitted power. This means that the majority of the power is scattered back rather than being transmitted in the fiber.

The threshold of HNLF-1145A corresponds to the point where the Brillouin scattered power turns to grow rapidly. From Fig. 2, the point is approximately 7 dBm which is in agreement with the calculated 6.67 dBm in Section 3.1.

4. Frequency resolution improvement with HNLF

HNLF-1145A and SMF-28 were experimentally characterized in a STFT-BOTDR setup as shown in Fig. 1. The signal after point C was heterodyned with the CW reference, whose polarization is rotating by using a polarization scrambler (PS), propagating and then down-

converted to the radio frequency (RF) range using a wideband photo-detector (PD), which is a 12 GHz high power InGaAs photodiode. The signal was amplified by a low noise amplified (LNA) which is used for SNR protection and was further down-converted to the intermediate frequency (IF) range by mixing with voltage control oscillator (VCO), and then the signal was digitized in the time domain and processed using the DFT signal processing algorithm to directly obtain the Brillouin spectrum peaks along the FUT [19,25-26], not the scanning method. The digitizer has a built-in 500 MHz low pass filter which has an asymmetric spectra shape. The normalized Brillouin scattering spectra of the two fibers were compared for a launched power of 13.3 dBm, as shown in Fig. 3. Both fibers were analyzed using 2500 averages, which correspond to a measurement speed of about 4 Hz. Particularly, in this experiment, the Brillouin spectrum peak frequency of HNLF-1145A and SMF-28 was down-converted to around 250 MHz and 235 MHz, respectively.

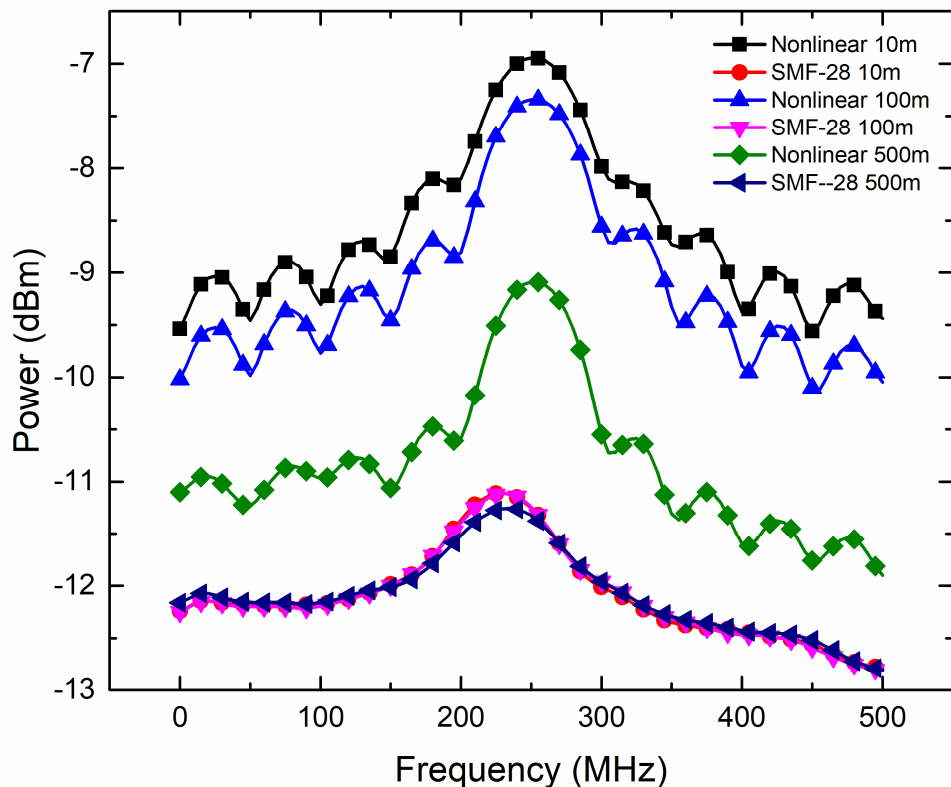


Fig. 3. Normalized spectra of the Brillouin scatter signal for the two FUT at 10 m, 100 m and 500 m location.

As previously discussed HNLF-1145A generated a much stronger Brillouin scattering spectrum and, thus, higher peak power at the BGS. The normalized plot in Fig. 3 shows that the spectrum peak to noise floor ratio is larger in HNLF-1145A comparing to SMF-28. Hence leading to a clear SNR improvement of the Brillouin scatter spectrum when HNLF-1145A was used. Note that the sidebands in the spectra are due to the larger nonlinear coefficients in the HNLF and further details are given in Section 5.

Figure 4 shows that the measured SNR in both fibers proportionally increases with the input power, between 4 dBm and 13 dBm. The SNR of HNLF-1145A grows from about 3 dB to about 13 dB, while the SNR of SMF-28 changes from about 1.5 dB to about 5 dB between this range. The slope of the curve for HNLF-1145A is twice than the one for SMF-28. It is

worth noting that the SNR is relative constant with the fiber length for the SMF-28 case, while it decreases when the fiber length increases for the HNLF-1145A case due to larger power attenuation. However, also in the worst case (500 m) the SNR of HNLF-1145A is still 6.5 dB higher than that of SMF-28 for an input power of 13 dBm. However, it is important to note that as the effective areas of the HNLF-1145A and SMF fiber are different, their corresponding power densities, defined as the ratio between power and effective area, in each fiber result in an intensity improvement of about 7 for the SMF case, with clear benefit in terms of SNR.

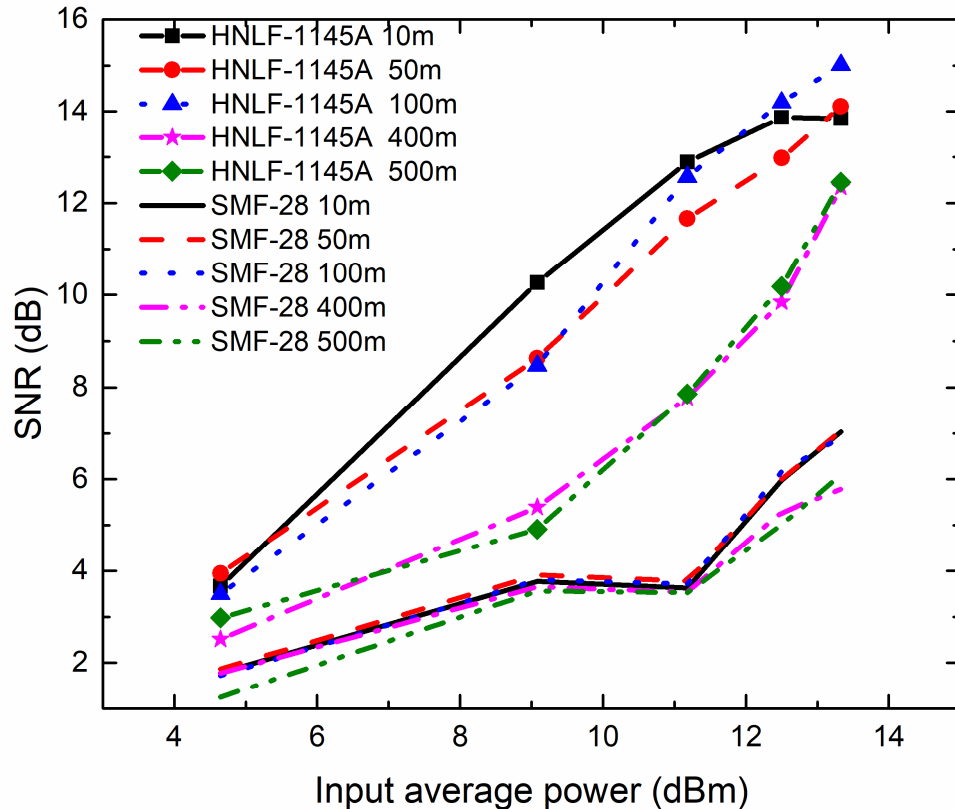


Fig. 4. The SNR for the HNLF-1145A and the SMF-28 at 10 m, 50 m, 100 m, 400 m, and 500 m locations along the fibers with different input power.

In the experiment, the two fibers were released with no changes in strain or temperature along their lengths. The Brillouin scattering peak power frequency was therefore assumed to remain constant in the fibers. Each measurement is the result of 2500 time averages. The accuracy tells the difference between the measured result and “true value”. Because the mean value of the measured frequency along the fibers can be considered as the true value, the frequency uncertainty represents the accuracy of the measurement. The frequency uncertainty can be calculated from the standard deviation of the peak frequencies along the fibers.

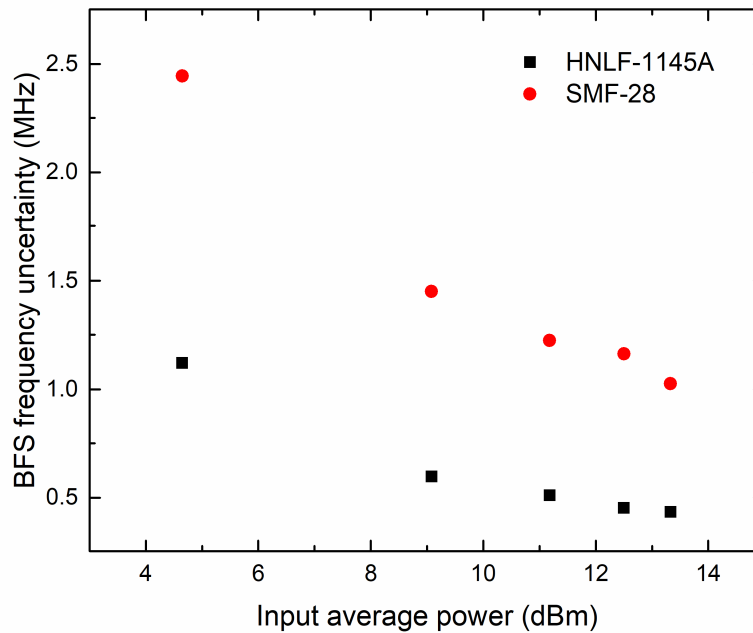


Fig. 5. The BFS uncertainty versus input average power for the HNLf-1145A and the SMF-28.

Figure 5 shows that the frequency uncertainty decreases as the incident average power increases, and that the frequency uncertainty for the HNLf-1145A case was about 2.5 times smaller than that of the SMF-28 case for all the studied incident powers. By using a measurement speed of 4 Hz, when the incident power was about 13.3 dB, the uncertainty was calculated to be about 0.43 MHz for HNLf-1145A, which corresponds to $10 \mu\epsilon$ or 0.43°C . The value would increase to about 1.02 MHz ($25 \mu\epsilon$ or 1.02°C) for SMF-28 using the same average number and conditions. The experimental results show the potential of highly nonlinear fibers for accurate distributed strain/temperature sensing.

5. Discussion on the use of HNLFs for sensing applications

Due to the larger nonlinear coefficients in HNLFs the transmitted seed suffers from nonlinear effects along its length, causing its spectrum to broaden and generate new spectral components. This effect causes the Brillouin scattering spectrum peak to deplete and drop, as it is demonstrated in Fig. 6 and will be discussed in the following section. When the launched pump power is 3.5 dBm (Fig. 6(a)), the peak power of the Brillouin scattering spectra in HNLf-1145A remains constantly with only about 1 dB drop from 10 m to 500 m. However, after 950 m, the peak power drops about 4 dB. This phenomenon of power reduction happens at shorter lengths when the launched pump power is increased. For example, when it is 7.87 dBm, the power dropped of about 10 dB after 400 m of propagation, see Fig. 6(b). Note that after the power drop at about 400m, it remains relative constant (1dB drop from 400 m to 500 m and about no change from 500 m to 900 m). Finally, when the incident pump power is as high as 12.30 dBm in Fig. 6 (c), the power drops about 4 dB in the first 100 m of propagation. Then it drops another 18 dB between 100 m to 400 m. Again, like the previous cases, after 400 m, the Brillouin scattering power remains constant with only small attenuation in the remaining fibers. It is worth noting that, even though the Brillouin scattering power suffers great power drops (after 400 m), it is still more than 10 dB higher than the Brillouin scattering power at the beginning of fiber when the incident pump power is only 3.5 dBm. This means that even with the high attenuation along the fiber when larger powers are used in the

BOTDR system, the corresponding Brillouin scattering power is still higher than the case of lower power.

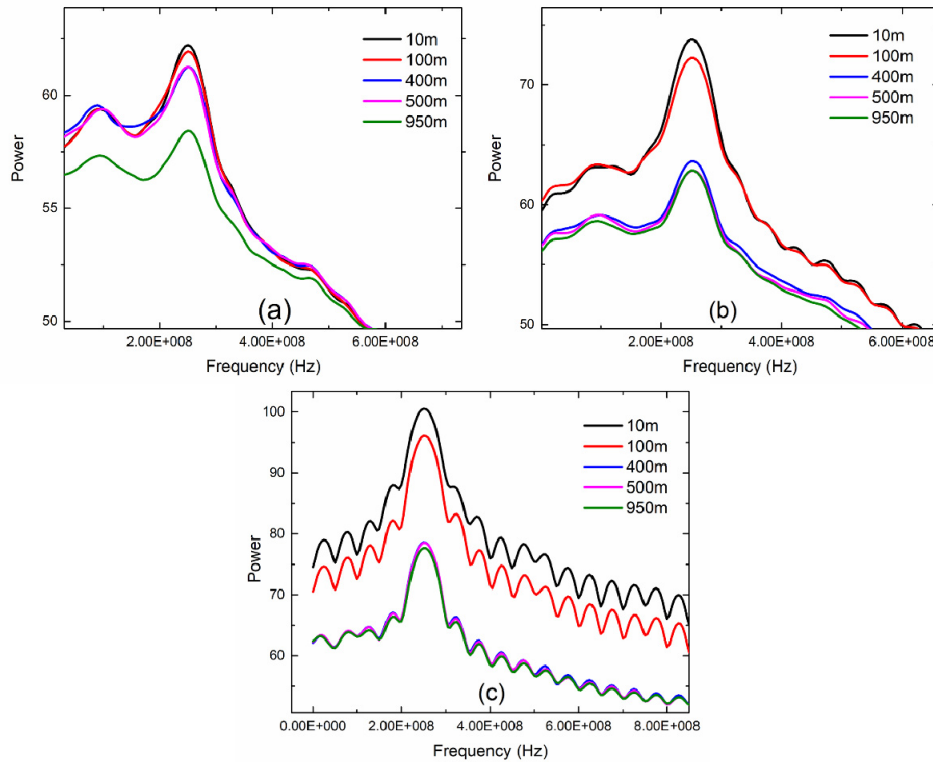


Fig. 6. The Power of the spectra of the HNLf-1145A fiber at position 10m, 100, 400m, 500m, 950m when the incident pump power is (a) 3.5 dBm, (b) 7.87 dBm, and (c) 12.30 dBm, vertical axis unit is relative value in dB.

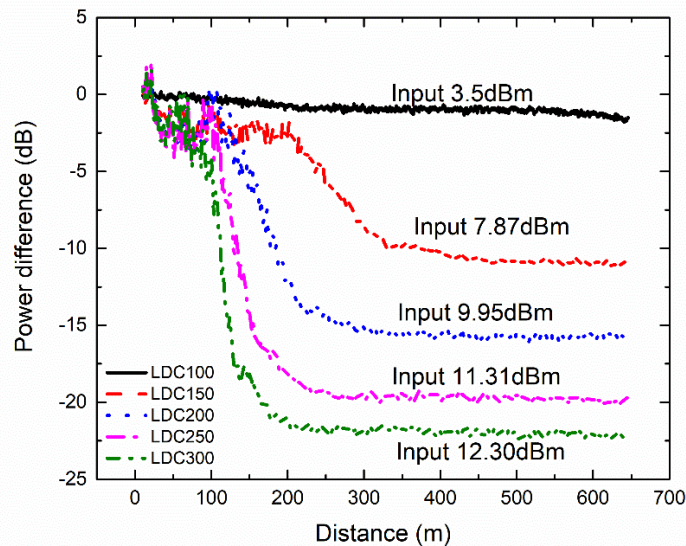


Fig. 7. The power difference of the launched power along the HNLf-1145A with input power 3.5 dBm, 7.87 dBm, 9.95 dBm, 11.31 dBm and 12.30 dBm.

The peak Brillouin scattering power along the fiber has been plotted in Fig. 7 for different launched powers. For each line, the starting point is used as reference point and set to be 0 dB. The peak power at each point along the fiber is compared to the launched power for all the cases. When the incident power is 3.5 dBm, according to Fig. 2, the fiber is in the SpBS region and the peak power shows no drops along the fiber. When the power is increased, the fiber is in SBS region, and it starts suffering peak power reduction (drop point) after certain distance. For example, in Fig. 7, the drop point moves from propagation lengths of 250 m to 100 m when the launched power increases from 7.87 dBm to 12.3 dBm. After the corresponding dropping points, we observe a “Linear Attenuation Section” where the power decreases almost linearly in dB. The drop distance shrinks while incident pump power grows, meaning that the power decreases faster when stronger SBS is generated.

In sight of the above improvements, HNLFs can potentially replace SMF-28 as they provide higher power Brillouin scattering and higher SNR with SBS enhancement under high incident pump power. Because of the relation between average number and SNR, by using HNLF, the average number can be reduced for each measurement. Therefore, the measurement speed can be improved for dynamic measurements [19].

6. Different HNLFs for BOTDR systems

As previously mentioned, the Brillouin power drop in HNLF-1145A is mainly a result of the power depletion due to modulation instability (MI), four-wave mixing (FWM) [16, 27] and self-phase modulation [28, 29] due to the high nonlinear coefficient of the fiber and anomalous dispersion ($\beta_2 < 0$). Different HNLFs with different fiber parameters, such as dispersion, need to be investigated by comparing their performances. We then used a second HNLF, HNLF-09, with similar effective area ($11.1 \mu\text{m}^2$), but normal dispersion (-1.7 ps/nm/km) to minimize the MI and FWM effects.

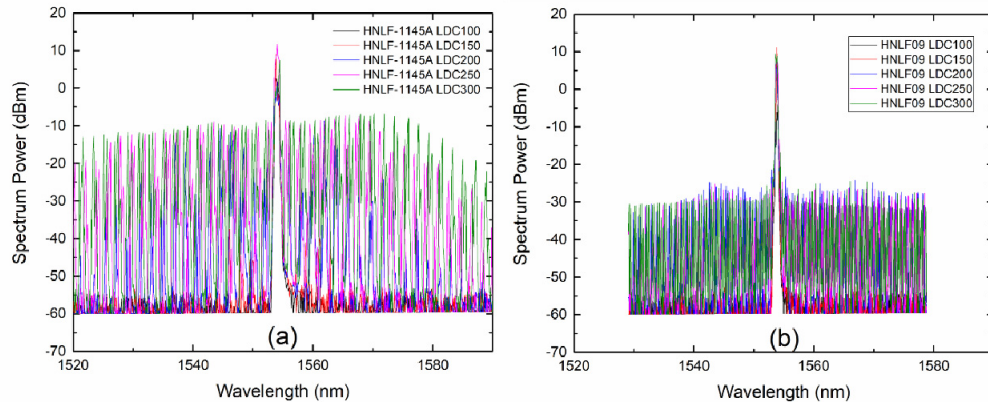


Fig. 8. Transmitted spectra at the end (1 km) of the HNLF-1145A (a) and HNLF-09 (b) when the incident pump power is 3.5 dBm (LDC100), 7.87 dBm (LDC150), 9.95 dBm (LDC200), 11.31 dBm (LDC 250), and 12.30 dBm (LDC300)

As predicted, looking at the transmitted spectra in the case of both HNLFs, the one with anomalous dispersion (HNLF-1145A) shows the generation of many harmonics (due to MI and FWM) symmetrically about the initial pump central wavelength causing it to deplete (see Fig. 8(a)). On the other hand, such nonlinear effects are minimized for the normal dispersive fiber (HNLF-09) and negligible pump depletion should occur (see Fig. 8 (b)).

Hence, the power drop in HNLF-09 will be smaller than HNLF-1145A and the pump light spectrum can be more stable in transmission. This is illustrated in Fig. 9, where the SNRs as a function of the fiber length are plotted for several launched powers for the two fibers. The SNRs of HNLF-09 is slightly smaller than the one of HNLF-1145A for the same launched

power at the beginning of the fibre length. However, since there is no power drop for HNLF-09 along its length towards the end of the fiber, the SNR actually becomes larger than the one of HNLF-1145A.

Normal HNLFs (HNLF-09) are therefore more suitable means for longer distance measurements. Anomalous HNLFs (HNLF-1145A) are more suitable where high frequency accuracy or very fast measurement speed are required but with the cost of shorter distance measurements.

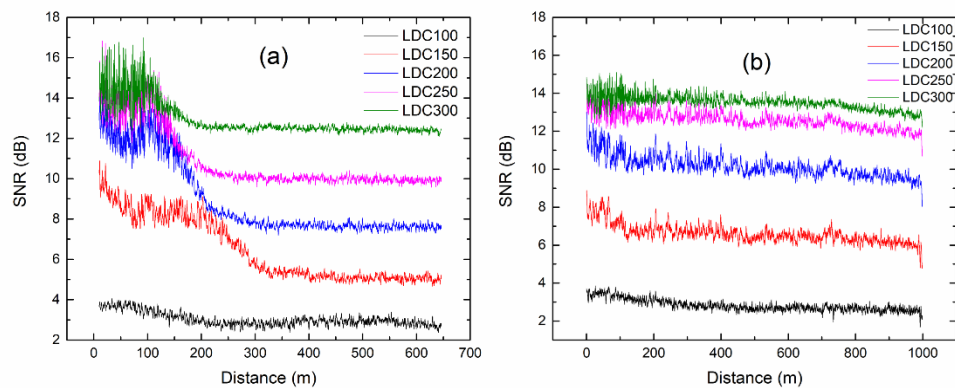


Fig. 9. The SNR along the HNLF-1145A (a) and HNLF-09 (b) when the incident pump power is 3.5 dBm (LDC100), 7.87 dBm (LDC150), 9.95 dBm (LDC200), 11.31 dBm (LDC 250), and 12.30 dBm (LDC300)

7. Conclusion

The Stimulated Brillouin scattering threshold of an anomalous highly nonlinear fiber HNLF has been measured and compared to the standard fiber SMF-28. Under the same launched pump power level, the power of Brillouin scattering in HNLF is higher than that in SMF.

The Brillouin scattering spectrum of HNLF-1145A has been experimentally studied in a STFT-BOTDR system and its performance was compared to that of SMF-28. The corresponding Brillouin spectrum bandwidth was 50 MHz for HNLF-1145A and 75 MHz for SMF-28. The SNR was approximately proportional to the incident power, and the frequency uncertainty in the HNLF-1145A case was about 2.5 times smaller than in the SMF-28 case. In this experiment, the best frequency uncertainty was 0.43 MHz, which is equivalent to 10 $\mu\epsilon$ in strain or 0.43°C in temperature with a measurement speed of 4 Hz.

The attenuation is more significant in HNLF-1145A than in HNLF-09. Results show that anomalous highly nonlinear fibers (e.g. HNLF-1145A) have the potential to be used in accurate strain/temperature sensing in both static and dynamic measurements, thanks to the high frequency accuracy and fast speed measurement. On the other hand, normal dispersive HNLFs (e.g. HNLF-09) have the potential to be used in relatively high frequency accuracy and long-distance measurement.

Funding

EPSRC (EP/P026575/1); EPSRC(EP/K000314/1).

Acknowledgement

The data for this work is accessible through the University of Southampton Institutional Research Repository. Linqing Luo and Bo Li are supported by the China Scholarship Council and Cambridge Commonwealth, European and International Trust.